THE JOURNAL OF BIOLOGICAL CHEMISTRY VOL. 285, NO. 29, pp. 22122–22131, July 16, 2010

Plastid-associated Porphobilinogen Synthase from *Toxoplasma gondii*

KINETIC AND STRUCTURAL PROPERTIES VALIDATE THERAPEUTIC POTENTIAL*[S]

Received for publication, January 25, 2010, and in revised form, April 19, 2010 Published, JBC Papers in Press, May 4, 2010, DOI 10.1074/jbc.M110.107243

Dhanasekaran Shanmugam[‡1], **Bo Wu**[‡1], **Ursula Ramirez**[§], **Eileen K. Jaffe**[§], **and David S. Roos**[‡2]

From the [‡]*Department of Biology, University of Pennsylvania, Philadelphia, Pennsylvania 19104 and the* [§]*Institute for Cancer Research, Fox Chase Cancer Center, Philadelphia, Pennsylvania 19111*

Apicomplexan parasites (including *Plasmodium* spp. and *Toxoplasma gondii*) employ a four-carbon pathway for *de novo* heme biosynthesis, but this pathway is distinct from the animal/fungal C4 pathway in that it is distributed between three compartments: the mitochondrion, cytosol, and apicoplast, a plastid acquired by secondary endosymbiosis of an alga. Parasite porphobilinogen synthase (PBGS) resides within the apicoplast, and phylogenetic analysis indicates a plant origin. The PBGS family exhibits a complex use of metal ions (Zn^{2+} and Mg^{2+}) and oligomeric states (dimers, hexamers, and octamers). Recombinant *T. gondii* PBGS (*Tg*PBGS) was purified as a stable ~320-kDa octamer, and low levels of dimers but no hexamers were also observed. The enzyme displays a broad activity peak (pH 7–8.5), with a K_m for aminolevulinic acid of ~150 μM and specific activity of ~24 μmol of porphobilinogen/mg of protein/h. Like the plant enzyme, *Tg*PBGS responds to Mg^{2+} but not Zn^{2+} and shows two Mg^{2+} affinities, interpreted as tight binding at both the active and allosteric sites. Unlike other Mg^{2+}-binding PBGS, however, metal ions are not required for *Tg*PBGS octamer stability. A mutant enzyme lacking the C-terminal 13 amino acids distinguishing parasite PBGS from plant and animal enzymes purified as a dimer, suggesting that the C terminus is required for octamer stability. Parasite heme biosynthesis is inhibited (and parasites are killed) by succinylacetone, an active site-directed suicide substrate. The distinct phylogenetic, enzymatic, and structural features of apicomplexan PBGS offer scope for developing selective inhibitors of the parasite enzyme based on its quaternary structure characteristics.

Heme is essential for cellular metabolism, and most organisms synthesize this tetrapyrrole cofactor *de novo*. Formation of aminolevulinic acid (ALA),[3] the first committed precursor in tetrapyrrole biosynthesis, is an important regulatory step in the pathway and is achieved differently in photosynthetic *versus* non-photosynthetic eukaryotes. The former use the "C5" pathway to adapt glutamyl tRNA using the enzymes glutamate tRNA reductase and glutamate semialdehyde aminomutase, whereas the latter use aminolevulinic acid synthase to condense glycine and succinyl coenzyme A via the "C4" pathway (1, 2). ALA is then converted into tetrapyrroles (heme, chlorophyll, B_{12}, etc.) using a multistep pathway, the first three enzymes of which are common to all organisms. In photosynthetic eukaryotes, the complete pathway for tetrapyrrole biosynthesis is located in the chloroplast, whereas in non-photosynthetic eukaryotes, the enzymes are typically distributed between the mitochondria and cytosol (1).

The first step in ALA utilization is catalyzed by the enzyme porphobilinogen synthase (PBGS; also known as δ-aminolevulinate dehydratase; EC 4.2.1.24), which converts two molecules of ALA into porphobilinogen (3). PBGS enzymes are highly conserved metalloproteins, with well documented enzymatic and structural properties (3, 4). Unusual characteristics include extensive variation in metal ion usage at the active and allosteric sites (5) and an unusually dynamic quaternary structure (6, 7). Cytosolic (animal/fungal) PBGS enzymes are Zn^{2+}-dependent, whereas the plastidic (plant/algal) PBGSs respond to Mg^{2+}. Sequence conservation and activity assays suggest that the latter contain two distinct Mg^{2+} binding sites: one presumed to be analogous to the catalytic Zn^{2+} in animal/fungal PBGS and an allosteric site present at an interdimer interface (5). Both the human (*Hs*PBGS) (7) and *Pisum sativum* (*Ps*PBGS) (6) enzymes exhibit allosteric regulation based on quaternary structure; homooctamers are highly active, whereas homohexamers are inactive; dissociation and conformational change at the dimer level is required for hexamer-octamer interconversion. Misregulation of the human PBGS quaternary structure equilibrium is associated with porphyric disease (8). Proteins exhibiting such alternative quaternary structure assemblies are called "morpheeins" (9).

The protozoan parasites *Plasmodium falciparum* and *Toxoplasma gondii* (both human pathogens in the eukaryotic phylum *Apicomplexa*) are capable of *de novo* heme biosynthesis, and inhibition of this pathway results in parasite death (10, 11). Phylogenetic studies reveal that apicomplexan heme biosyn-

* This work was supported, in whole or in part, by National Institutes of Health Grants AI28724 (to D. S. R.), ES003654 (to E. K. J.), T32CA00935 (to the Institute for Cancer Research), AI077577 (to E. K. J.), and CA006927 (to Fox Chase Cancer Center).

[S] The on-line version of this article (available at http://www.jbc.org) contains supplemental Tables S1 and S2, Text S1, and Figs. S1 and S2.

[1] Both authors contributed equally to this work.

[2] To whom correspondence should be addressed. E-mail: droos@sas.upenn.edu.

[3] The abbreviations used are: ALA, aminolevulinic acid; eGFP, enhanced green fluorescent protein; PBGS, porphobilinogen synthase; *Hs*PBGS, *H. sapiens* PBGS; *Ps*PBGS, *P. sativum* PBGS; *Pa*PBGS, *P. aeruginosa* PBGS; *Tg*PBGS, *T. gondii* PBGS; RACE, rapid amplification of cDNA ends; SPP, stromal processing protease (pitrilysin); *Tg*SPP, T. gondii SPP; Bistris propane, 1,3-bis[tris(hydroxymethyl)methylamino]propane; GFP, green fluorescent protein; β-ME, β-mercaptoethanol.

thesis enzymes exhibit a mosaic of plant and animal origins and are distributed between the parasite mitochondrion, plastid (apicoplast), and cytosol (12, 43). The plastid-associated enzymes are of plant origin, and plastid PBGS is sufficiently distinct from human PBGS to offer potential as a therapeutic target. *P. falciparum* PBGS forms active octamers and exhibits an unusual metal ion-independent activity (13).

In this report, we describe the cloning of multiple cDNAs encoding *T. gondii* PBGS (*Tg*PBGS), identification and expression of the physiologically relevant isoform, and kinetic characterization of this enzyme. Unlike *Ps*PBGS and *Pseudomonas aeruginosa* PBGS (*Pa*PBGS), Mg^{2+} is not required for *Tg*PBGS octamer stability, which appears to be conferred by an unusual C-terminal amino acid extension found in all apicomplexan PBGSs.

MATERIALS AND METHODS

Molecular Procedures—A Lambda Zap II *T. gondii* cDNA library (11) was used to PCR-amplify various fragments of the *Tg*PBGS gene (see supplemental Table S1 for a list of primers), and full-length cDNA sequences were obtained by a combination of library screening and rapid amplification of cDNA ends (RACE). Quantitative "real-time" PCR of *Tg*PBGS and *T. gondii* stromal processing peptidase (*Tg*SPP) transcripts was carried out using poly(A)$^+$ mRNA and the Power SYBR Green kit (Applied Biosystems); absolute levels were determined based on amplification of standards over a range of concentrations from 1 fg to 100 pg. Bradyzoite and sporozoite RNA was kindly provided by Drs. Florence Dzierszinski (McGill University) and Michael White (University of South Florida), respectively. A recombinant fragment of *Tg*PBGS (amino acids 363–658) fused to a C-terminal His tag was expressed in *Escherichia coli*, purified on Ni^{2+}-agarose beads (Qiagen), and used to prepare mouse polyclonal antiserum (Cocalico Inc.) for Western blotting and immunofluorescence according to standard protocols. See below for production and purification of recombinant enzyme.

Parasite Cultures—RH strain *T. gondii* tachyzoites were used throughout this study, following standard methods to propagate parasites in primary human foreskin fibroblast cell monolayers (14). Freshly isolated parasites were used to obtain genomic DNA (Roche Applied Science High Pure PCR template preparation kit) and total RNA (Qiagen RNeasy$^+$ minikit) according to the manufacturers' protocols. Parasites, expressing firefly luciferase under control of the β-tubulin promoter (15), were employed for growth and inhibition assays.

TgPBGS Localization and Transit Peptide Cleavage—Transgenic parasites were engineered to express an N-terminal fragment of *Tg*PBGS (amino acids 1–394; Fig. 1*E*) driven by an upstream β-tubulin promoter and fused to either enhanced green fluorescent protein (eGFP) (for subcellular localization) or hemagglutinin-tagged glutathione *S*-transferase (for mapping the transit peptide cleavage site). Tachyzoites transiently transfected with the $TgPBGS_N$-eGFP plasmid (14) were incubated 18 h prior to fixation in 3.7% paraformaldehyde, permeabilization with 0.25% Triton X-100, and staining with polyclonal rabbit anti-*T. gondii* acyl carrier protein (43) followed by Alexa fluor-594 goat anti-rabbit IgG (Invitrogen). DNA was stained by a 5-min incubation in 2.8 μM 4′,6-diamidino-2-phenylindole dye, and imaging was carried out on an Olympus IX70 inverted microscope equipped with a mercury vapor lamp, appropriate barrier/emission filters (DeltaVision), and a Photometrics CoolSNAP high resolution digital CCD camera.

A stable transgenic parasite line expressing $TgPBGS_N$-glutathione *S*-transferase-hemagglutinin protein was obtained using standard methods for chloramphenicol selection and clonal isolation (14). Protein was purified from a lysate of 10^{10} transgenic parasites using glutathione-coupled agarose beads (Amersham Biosciences), separated by SDS-PAGE, and stained with SimplyBlue SafeStain (Invitrogen), and the mature protein band was excised for N-terminal protein sequencing (Cambridge Peptides Inc.).

Purification of Recombinant TgPBGS—cDNA clones of wild type *Tg*PBGS (amino acids 303–658, including all conserved PBGS sequences and the C terminus) or *Tg*PBGS-ΔC (amino acids 303–645; lacking the 13-amino acid apicomplexan-specific C-terminal extension; see Fig. 1*E*) were cloned into expression vector *p*ET3a (Stratagene) and used to transform *E. coli* BLR(DE3) cells. Single colonies were inoculated into 1 liter of LB media containing 100 μg/ml ampicillin, 12.5 μg/ml tetracycline, and 0.4% glucose; incubated 12 h at 37°C in a shaking incubator; pelleted and resuspended in 1 liter fresh LB without glucose; and equilibrated to 15 °C. Protein expression was induced by the addition of 100 μM isopropyl 1-thio-β-D-galactopyranoside and allowed to proceed for 15 h, followed by centrifugation at 4 °C to harvest. A 10-g pellet was resuspended in 20 ml of buffer containing 0.4 mg/ml lysozyme (Sigma), 50 mM KH_2PO_4, pH 8.0, 170 mM KCl, 5 mM EDTA, 10 mM β-ME, and 0.1 mM phenylmethylsulfonyl fluoride. After stirring for 20 min, this mixture was diluted 1:1 with 20 ml of 100 mM KH_2PO_4, pH 7.0, 12 mM $MgCl_2$, 40 μM $ZnCl_2$, 10 mM β-ME, and 0.1 mM phenylmethylsulfonyl fluoride, followed by the addition of DNase I (Sigma) to a final concentration of 25 μg/ml and a 20-min incubation at 25 °C with stirring.

Bacteria were lysed by several cycles of freezing, thawing, and sonication and sequentially precipitated using a cut between 20 and 45% ammonium sulfate. *Tg*PBGS protein precipitated in the 45% pellet and was resuspended in 30 mM KH_2PO_4, pH 7.5, 5% ammonium sulfate, and 0.1 mM $MgCl_2$. The protein was applied to a 75-ml phenyl-Sepharose CL-4B column (GE Healthcare) and eluted at 4 °C using a 750-ml gradient from 30 to 2 mM KH_2PO_4 (pH 7.5) and from 15 to 0% ammonium sulfate, in the presence of 0.1 mM $MgCl_2$. 10-ml fractions were collected at a flow rate of 1 ml/min, and those containing enzyme activity were pooled and applied to a 75-ml Q-Sepharose column (GE Healthcare) equilibrated with 10 mM Tris, pH 7.0, and 1 mM $MgCl_2$. The column was eluted at room temperature using a 1-liter Tris gradient from 10 mM to 1 M at pH 7 in the presence of 1 mM $MgCl_2$. 10-ml aliquots were collected at 3 ml/min, and those spanning the enzyme activity peak were pooled based on purity (assessed by SDS and native gel electrophoresis) and concentrated to ~6 mg/ml. A 24-ml Superdex 200 analytical gel filtration column (GE Healthcare) equilibrated in 100 mM Tris, pH 7.0, 1 mM $MgCl_2$, 10 mM β-ME was used to determine protein size after calibration with standard markers. All chromatography columns were run using the

AKTA system (GE Healthcare). A portion of the resulting *Tg*PBGS protein was dialyzed against several changes of 10 mM Tris, pH 7, containing 10 mM β-ME to remove Mg^{2+} ions.

Monitoring Parasite Heme Synthesis by ^{14}C-ALA Incorporation—Freshly isolated, extracellular tachyzoite stage parasites were washed and resuspended in minimal essential medium (Invitrogen) containing 1% dialyzed fetal calf serum. 10^8 parasites were preincubated for 2 h at 37 °C under 5% CO_2 in 1 ml of minimal essential medium containing 0, 0.1, 0.25, 0.5, 1, or 2 mM succinylacetone (pH 7.3), followed by the addition of 1 μCi of ^{14}C-ALA (HCl salt) and incubation for a further 6–8 h. Radiolabeling was stopped by centrifugation and washing with fresh minimal essential medium. Heme was extracted as described previously (16), and radioactivity was estimated by scintillation counting.

Enzyme Activity Assays—PBGS assays were run in 100 mM Bistris propane-HCl buffer containing 10 mM β-ME, as previously reported (17), using 10 μg/reaction protein except when testing protein concentration dependence. Reaction mixtures were preincubated at 37 °C for 10 min before starting the assay with the addition of ALA (10 mM unless otherwise stated). Assays were typically run for 20 min, followed by the addition of 0.1 M $HgCl_2$ in 20% trichloroacetic acid, development for 8 min in Ehrlich's reagent, and measurement of absorbance at 555 nM using the quartz dip probe on a Cary50 spectrometer. Enzyme activity was measured in parasite lysates using 200 μg of total protein (~10^8 parasites) per assay and a 1-h reaction time.

Homology-based Structural Model of TgPBGS—The *Pa*PBGS crystal structure (Protein Data Bank entry 1GZG) was used as a template for constructing a structural homology model of *Tg*PBGS amino acids 324–643. Alignments were constructed in MolIDE (18) using PSI-BLAST (≥47% identity). Gaps in the alignment map to loops and were modeled independently for each monomer using Loopy (19). Side chain coordinates were retained from the template structure for identical residues; non-identical side chains were modeled using SCWRL 3.0 (20). Side chains for each subunit of the octamer were modeled in the presence of the other subunits to impart appropriate conformational constraints. *Pa*PBGS forms an octamer in solution, and the crystal structure contains two monomers in its asymmetric dimeric unit. The *Tg*PBGS octamer was therefore modeled using one template monomer for subunits A, C, E, and G and the other for subunits B, D, F, and H.

Because no template crystal structure is available for the C-terminal extension of apicomplexan PBGS, *Tg*PBGS(644–658) (VEDMKGTQKFTEPCY) was modeled based on similar sequences in other proteins. The Protein Data Bank provides at least nine sequences (32 structures) containing ≥5 conserved and ≥4 identical amino acids. Five proteins include the sequence VEDMK, which is always helical. The sequence GTQKFT forms a loop and helix in several structures. In three different protein families containing the sequence FTEPCY, PCY was always a non-helical, non-strand loop region, and FTE was variable. Secondary structures for each subsequence were combined using ϕ-ψ angles from available crystal structures, and examination of the resulting possibilities produced only two sterically feasible combinations, one of which was clearly superior based on its interface with the rest of the *Tg*PBGS model. This structure was added to each subunit of the dimer model, with manual adjustment to remove steric hindrance and improve the interaction surface with the two monomeric units. The resulting model was then overlaid with each of the dimers of the octameric 1GZG to form an octamer model of *Tg*PBGS. The protein preparation workflow in Maestro (Schrödinger, LLC) was used to add hydrogen atoms and identify overlapping atoms in the octameric structure, and the entire model was manually refined to accommodate all interfacing residues. The quality of the resulting model was estimated using the Protein Interfaces, Surfaces, and Assemblies Service (21). See supplemental Text T1 for PDB coordinates of the *Tg*PBGS structure model.

RESULTS

Genomic Organization and Expression of T. gondii PBGS Gene—Analysis of the *T. gondii* ME49 reference genome (see the ToxoDB Web site) identifies a single candidate PBGS gene, on chromosome III (TGME49_053900). Few expressed sequence tags map to this locus, and microarray evidence suggests low transcript abundance, but several independent proteomic studies have identified *Tg*PBGS peptides (see the ToxoDB Web site). A combination of library screening and reverse transcription-PCR revealed four alternatively spliced transcripts defining 17 exons (Fig. 1*A*). *Tg*PBGS1 (DQ029337, 3863 nucleotides) fuses exons 1-2-4-5-6-7; *Tg*PBGS2 (DQ029338, 3641 nucleotides) fuses exons 1-3-4-5-6-7, using an alternative splice donor and acceptor that truncate exons 1 and 3; *Tg*PBGS3 (DQ029339, 4579 bp) transcripts appear to initiate 129 nucleotides upstream of *Tg*PBGS1 and -2 and fuse exons 1-2-3-4-5-6-7. All three of these transcripts include conserved PBGS sequences. The fourth cDNA includes no mature PBGS sequence, fusing exons 1 and 2 to exons 8–17 (confirmed by reverse transcription-PCR using primer pairs, as indicated in Fig. 1*A*, and by RACE; not shown) and is predicted to encode a plastid stromal processing peptidase (*Tg*SPP). Production of these two unrelated proteins from the same genetic locus is also observed in *P. falciparum* (22). Quantitative real-time PCR was used to calculate steady-state abundance of *Tg*PBGS in RH strain tachyzoites as 155.2 ± 31.3 fg/μg of poly(A)$^+$ mRNA, *versus* 44.7 ± 2.2 fg/μg for *Tg*SPP (*i.e.* *Tg*PBGS is 3.45 ± 0.53-fold more abundant than *Tg*SPP) (Fig. 1*B*).

Sequences upstream of the first four ATGs differ from the consensus translational start site for *T. gondii* (caaaATG) 23), are not conserved in the related parasite *Neospora caninum* (see the ToxoDB Web site), and fail to initiate a long open reading frame, but the fifth ATG permits synthesis of proteins of 462, 658, or 1715 amino acids (for *Tg*PBGS1, *Tg*PBGS3, and *Tg*SPP, respectively). Use of the fourth ATG would correct for the frameshift introduced by *Tg*PBGS2 intron 1, yielding an open reading frame of 407 amino acids. Only *Tg*PBGS3 is predicted to encode all conserved PBGS sequences (exons 3–7), and Northern blot hybridization reveals a 4.6-kb *Tg*PBGS3 mRNA (not shown). Similarly, Western blotting using polyclonal mouse antiserum raised against *Tg*PBGS (see "Materials and Methods") detected a ~56-kDa protein (Fig. 1*C*), larger than the predicted size of *Tg*PBGS1 or -2 but consistent with

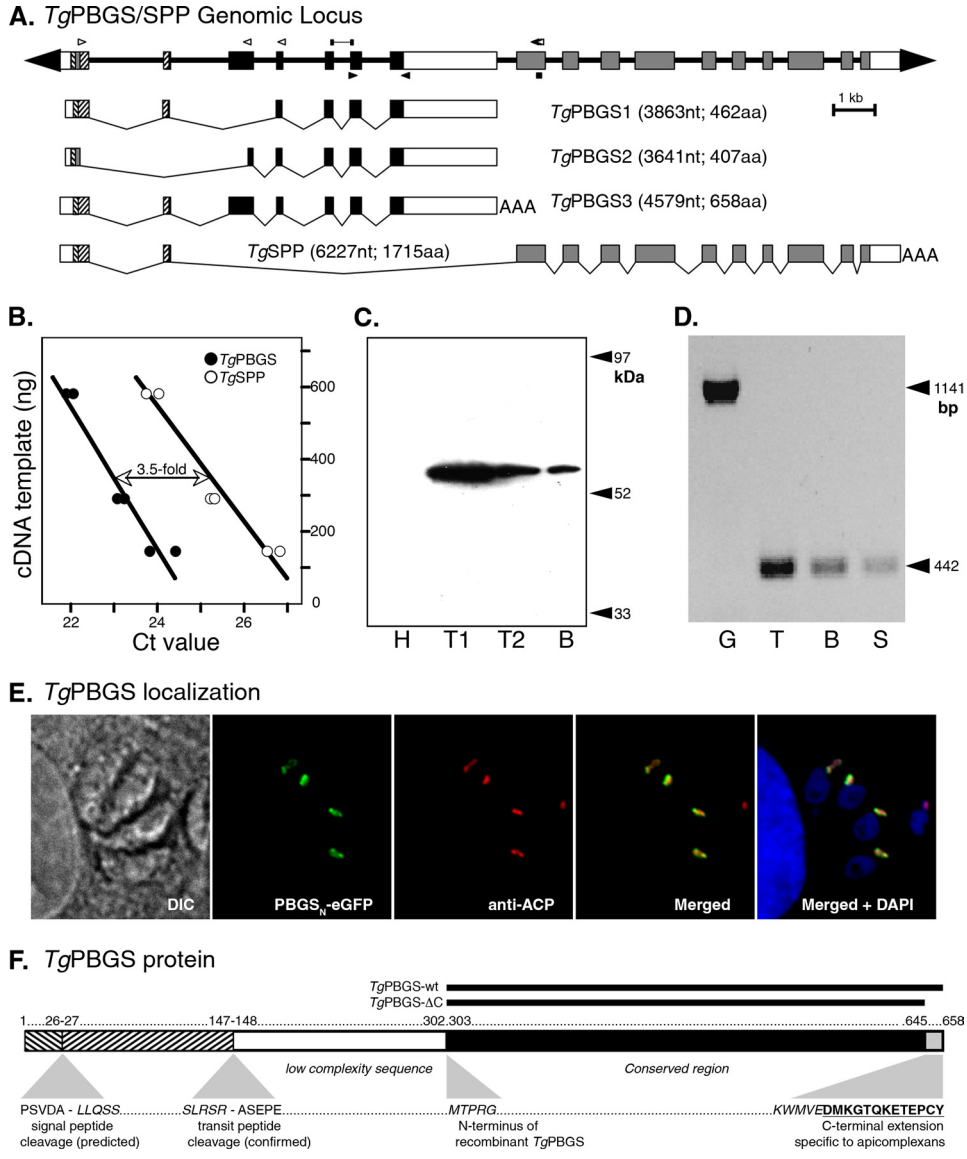

FIGURE 1. ***Tg*PBGS organization, expression, and localization.** *A*, 23 kb spanning the *T. gondii* PBGS/SPP locus on chromosome III. Exons 1 and 2 encode a bipartite apicoplast-targeting signal (signal sequence + plastid-targeting domain; *hatched boxes*), fused to mature coding sequences for *Tg*PBGS (exons 3–7; *black boxes*) or *Tg*SPP (exons 8–17; *gray boxes*). The *white boxes* indicate 5′- and 3′-untranslated regions (precise polyadenylation sites have not been mapped for *Tg*PBGS1 and -2). The *open arrowheads* indicate primers used to define the 5′-end of *Tg*PBGS and *Tg*SPP transcripts by reverse transcription-PCR or RACE, *bars* indicate fragments amplified for quantitative PCR analysis of mRNA abundance, and *closed arrowheads* indicate primers used for assessing *Tg*PBGS expression in different parasite stages. Three distinct transcripts including PBGS sequences were identified. *B*, quantitation of *Tg*PBGS and *Tg*SPP transcripts by quantitative real-time PCR using gene-specific primer pairs (supplemental Table S1); *Tg*PBGS was amplified above the *Ct* threshold ~2 cycles earlier than *Tg*SPP, corresponding to a 3.5-fold difference in mRNA abundance (replicate samples at three different dilutions). *C*, Western blotting of parasite cell lysates detects the 56-kDa PBGS3 protein. *H*, primary human foreskin fibrobast host cell lysate; *T1*, 5×10^6 *T. gondii* tachyzoites; *T2*, 10^6 tachyzoites; *B*, 400 *T. gondii* bradyzoite cysts (purified from a chronically infected mouse brain). *D*, a 442-bp PCR product specific for *Tg*PBGS3 mRNA was detected in tachyzoites (*T*), bradyzoites (*B*), and sporozoites (*S*). *G*, amplification of genomic DNA using the same primers yields a 1.1-kb product. *E*, subcellular localization of *Tg*PBGS in transgenic parasites expressing the N-terminal leader (394 amino acids) fused to eGFP (*green*). The apicoplast (*red*) was detected by immunostaining for *T. gondii* acyl carrier protein (*ACP*). 4′,6-diamidino-2-phenylindole (*DAPI*) (*blue*) stains the apicoplast and both parasite and host cell nuclei. *DIC*, differential interference contrast. *F*, schematic diagram of *Tg*PBGS protein features showing the bipartite plastid-targeting region (*hatched*), predicted signal peptide, and experimentally determined transit peptide cleavage sites and the portions expressed as recombinant proteins. *aa*, amino acids; *nt*, nucleotides.

the predicted size of *Tg*PBGS3 after cleavage of the apicoplast-targeting signal. *Tg*PBGS transcripts were detected in cDNA derived from three major parasite life cycle stages: tachyzoites, bradyzoites, and sprozoites (Fig. 1*D*).

Subcellular Localization and Mapping the Correct N-terminal Region of Mature TgPBGS—Exons 1 and 2 are predicted to encode a bipartite apicoplast-targeting signal (24), consisting of a secretory signal sequence fused to a plastid-targeting domain, and are presumed to target both PBGS and SPP to the apicoplast (22). We confirmed apicoplast targeting of *Tg*PBGS3 by expressing the N-terminal 394 amino (derived from exons 1–4) fused to eGFP in a transgenic parasite line (see "Materials and Methods" and supplemental Table S1 for primers). Co-localization with a validated marker (acyl carrier protein) (43) confirmed apicoplast localization (Fig. 1*E*). In order to precisely map the transit peptide cleavage site, thereby defining the correct N terminus of mature *Tg*PBGS, a cDNA encoding the same N-terminal leader sequence was expressed in *T. gondii* tachyzoites as a C-terminal glutathione *S*-transferase-hemagglutinin fusion. This protein was isolated from parasite lysates using glutathione-Sepharose beads, and its N-terminal sequence was determined by mass spectrometry. The mature N terminus begins with alanine 184, after cleavage between positions 183 and 184 ($SSLRSR^{183} \downarrow A^{184}SEP$), as shown in Fig. 1*F*. Starting from Ala^{184}, only *Tg*PBGS3 mRNA would be capable of encoding the ~56-kDa (510 amino acids) mature protein detected by Western blotting (Fig. 1*C*).

Cloning and Purification of Recombinant TgPBGS—In order to study its kinetic properties, a recombinant version of the enzyme encoded by *Tg*PBGS3 was overexpressed and purified from *E. coli* (see "Materials and Methods"). *Tg*PBGS-wt (Fig. 1*F*) excludes the N-terminal targeting signals (amino acids 1–147) and low complexity sequence (amino acids 148–301), but includes amino acids 303–658 spanning all conserved PBGS sequences and a C-terminal extension that distinguishes apicomplexan PBGS from most other species (see supplemental Fig. S1). A mutant *Tg*PBGS lacking the C-terminal 13 amino acids was also engineered (*Tg*PBGS-

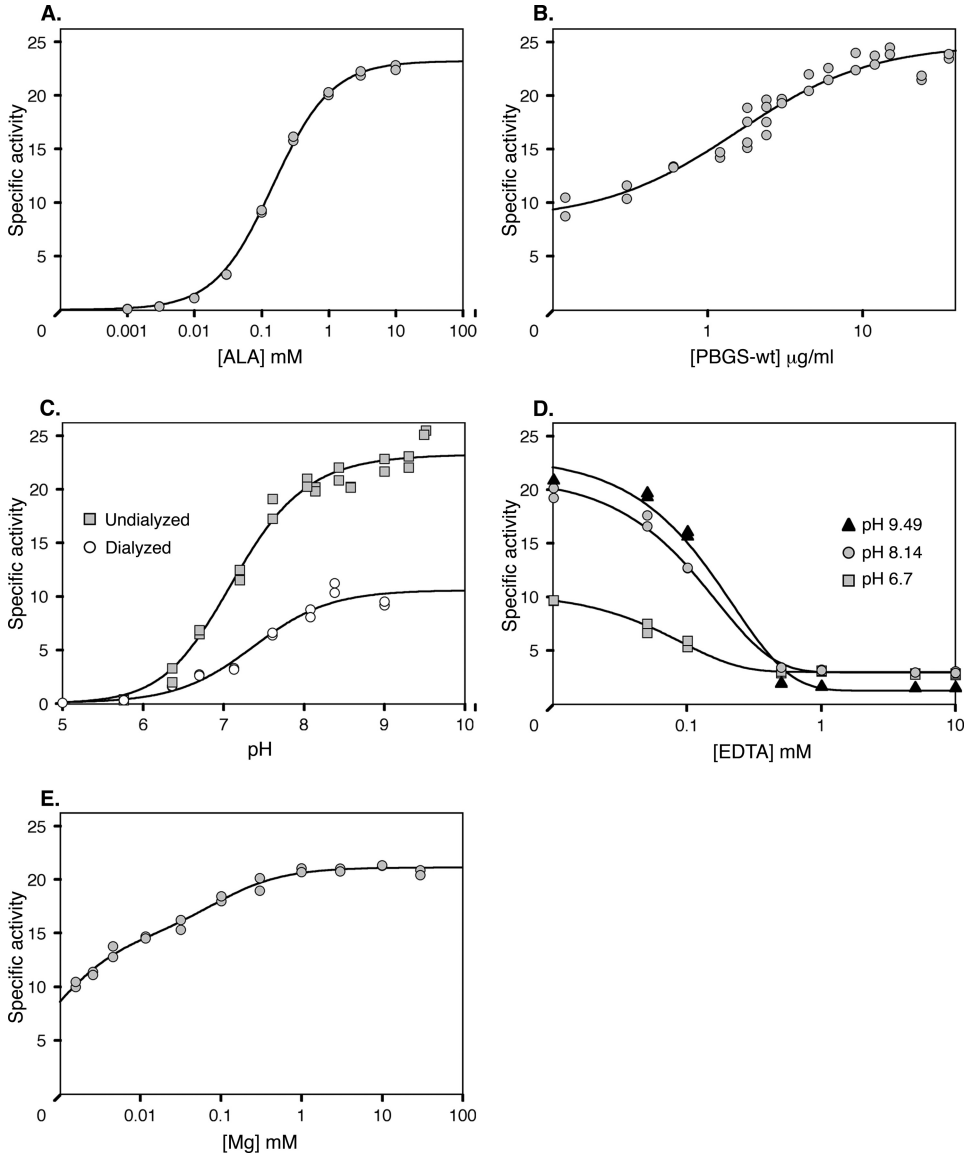

FIGURE 2. **Kinetic properties of wild type *Tg*PBGS.** *A*, specific activity as a function of ALA concentration. Fitting to the Michaelis-Menten equation yields a K_m value of 0.149 mM and V_{max} of 23.2 μmol porphobilinogen/mg of protein/h. *B*, *Tg*PBGS specific activity is dependent on enzyme concentration, reaching maximal activity at ~10 μg/ml (~0.25 μM). The data are fitted to a simple hyperbolic equation with a y (offset). *C*, specific activity of *Tg*PBGS as a function of pH and Mg^{2+}. Undialyzed protein (*squares*) contains ~2 μM Mg^{2+}, and dialyzed protein (*circles*) contains <0.01 μM Mg^{2+}; ALA contributed an additional ~0.18 μM Mg^{2+} to the assay. *D*, effect of EDTA on *Tg*PBGS enzyme activity (using undialyzed *Tg*PBGS without added Mg^{2+}). *E*, $MgCl_2$ titration of *Tg*PBGS specific activity. Two K_d values of ~0.7 and 84 μM were determined, based on fitting a double hyperbolic equation. Unless otherwise specified, standard assay conditions included 10 μg/ml *Tg*PBGS (except in *B*), 10 mM ALA (except in *A*), pH 8.14 (except in *C* and *D*), 1 mM $MgCl_2$ (except in *C–E*), and 10 mM β-ME; assays were initiated by the addition of ALA and incubated for 20 min at 37 °C.

ΔC; Fig. 1*F*) in order to compare its native structure and kinetic properties with the wild type enzyme.

*Tg*PBGS-wt activity eluted as a single peak from a phenyl-Sepharose column (supplemental Fig. S2*A*, *top left*), yielding 90 ml of pooled fractions at ~1 mg/ml protein. Subsequent fractionation of the phenyl-Sepharose peak on Q-Sepharose (supplemental Fig. S2*A*, *top right*) provided a 40-ml pooled fraction volume of enzyme activity peak at ~1.2 mg/ml. All column buffers contained 1 mM $MgCl_2$ (see "Materials and Methods" and supplemental Table S2 for further purification details). *Tg*PBGS-ΔC activity eluted from the phenyl-Sepharose column with a slightly extended shoulder before the peak, and the partially purified protein displayed a broad elution profile from Q-Sepharose (supplemental Fig. S2*A*, *bottom*). The size and purity of recombinant proteins were confirmed by SDS-PAGE (supplemental Fig. S2*B*); because *Tg*PBGS-ΔC exhibits very low activity, positive fractions were pooled and concentrated. Purified *Tg*PBGS-ΔC protein formed a fluffy precipitate upon extended storage. No contaminating *E. coli* PBGS was detected (25), based on assays of *Tg*PBGS-ΔC phenyl-Sepharose peak without metals, with Zn^{2+} alone, Mg^{2+} alone, or Zn^{2+} plus Mg^{2+} (data not shown).

Kinetic Properties and Metal Ion Dependence of Recombinant TgPBGS—Under optimal conditions (see "Materials and Methods"), the wild type *Tg*PBGS enzyme exhibits specific activity of 23–25 μmol of porphobilinogen/mg of protein/h and a K_m of 0.149 mM (Fig. 2*A*), comparable with previous reports for PBGS from other species (7, 17, 26, 27). *Tg*PBGS activity is also dependent on protein concentration, reaching maximal activity at ~10 μg/ml (~0.25 μM) and an apparent K_d of ~0.04 μM (Fig. 2*B*), comparable with values reported for *Ps*PBGS (17) and *Bradyrhizobium japonicum* PBGS (26). In other systems, concentration dependence is associated with regulation based on quaternary structure because high protein concentration favors the formation of high activity octamers over low activity hexamers. The specific activity of *Tg*PBGS does not approach zero at low protein concentrations, however, suggesting a different quaternary structure equilibrium. The excellent fit to standard Michaelis-Menten kinetics over substrate concentrations from 1 μM to 10 mM (Fig. 2*A*) also argues against alternative quaternary structure assemblies with differing K_m values (6, 29).

Many PBGS enzymes are completely dependent on metal ions, but some Mg^{2+}-binding enzymes exhibit partial metal ion independence (13, 30). Because protein sequence alignments suggested that *Tg*PBGS can bind Mg^{2+} at both the active site and an allosteric site, the enzyme was purified in 1 mM Mg^{2+} (see "Materials and Methods"). Close to maximal activity was observed using undialyzed *Tg*PBGS-wt in assays containing ~2 μM Mg^{2+} (Fig. 2*C*, *squares*). Thus, if Mg^{2+} is required for activ-

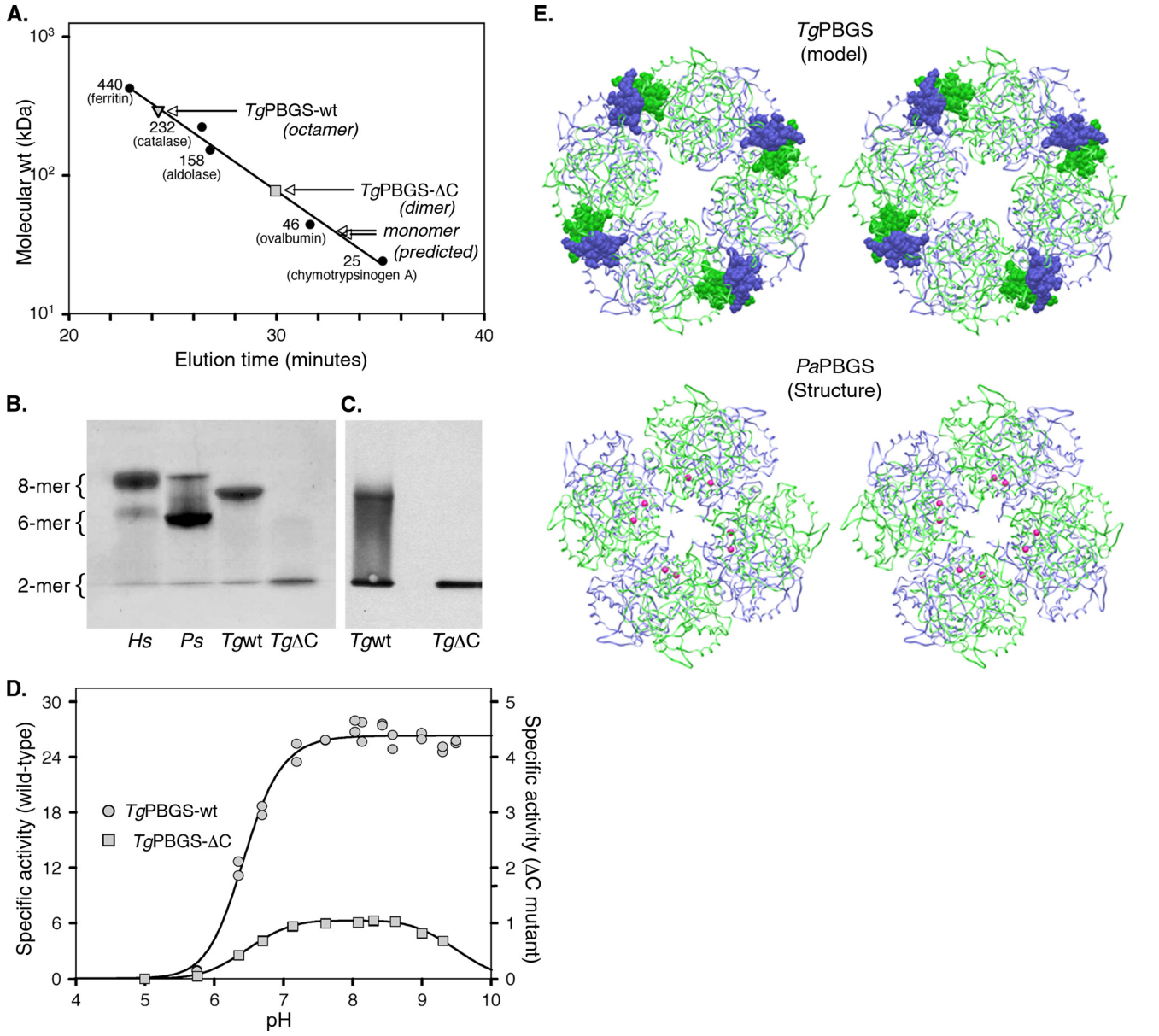

FIGURE 3. **Quaternary structure analysis of *Tg*PBGS-wt and *Tg*PBGS-ΔC.** *A*, determination of molecular mass by gel filtration chromatography on Superdex 200 (0.1 M Tris, pH 8.5, 10 mM $MgCl_2$, 10 mM β-ME, 0.2 M NaCl). Enzyme elution was assessed at A_{280}, and the column was calibrated using size markers as shown (Amersham Biosciences). For comparison, the expected elution times for monomeric *Tg*PBGS-wt and *Tg*PBGS-ΔC are also indicated. *B*, native PAGE analysis of *Hs*PBGS (octamer > hexamer ≫ dimer), *Ps*PBGS (hexamer > octamer ≫ dimer), *Tg*PBGS-wt (octamer ≫ dimer), and *Tg*PBGS-ΔC (dimer only). *C*, Western blotting (of native gels) confirms that the *Tg*PBGS-ΔC mutant fails to form octamers. Comparison with *B* suggests that this antibody displays higher affinity for the dimer than the octamer form of *Tg*PBGS. *D*, activity profile demonstrates ~25-fold lower specific activity for *Tg*PBGS-ΔC relative to *Tg*PBGS-wt (0.1 M Bistris propane, 1 mM $MgCl_2$, 10 mM β-ME, 10 mM ALA; pH range as indicated). *E*, homology model of *Tg*PBGS octamer (*top*) and crystal structure of *Pa*PBGS octamer (Protein Data Bank entry 1GZG; *bottom*), displayed as *stereo images*. *Green*, subunits A, C, E, and G; *blue*, subunits B, D, F, and H. *Magenta*, allosteric magnesium ions stabilizing the octamer form of *Pa*PBGS. *Tg*PBGS octamers are stable even in the absence of magnesium, probably because of dimer-dimer interactions mediated by the C-terminal extension unique to apicomplexan parasites (amino acids 646–658; shown in *CPK*).

ity, it has a very high affinity for the protein because the binding site seems to be significantly populated even at low Mg^{2+} concentrations. ~40% maximal activity was detected even after dialysis depleted Mg^{2+} to <0.3 ions/octamer, as determined by atomic absorption spectroscopy (Fig. 2*C*, *circles*). EDTA treatment eliminated the activity of undialyzed protein (Fig. 2*D*), consistent with the hypothesis of a tight binding catalytic Mg^{2+}. Varying the concentration of Mg^{2+} added to the reaction suggests two affinities, with K_d values of ~0.7 and 84 μM (Fig. 2*E*), which we attribute to the active and allosteric sites, respectively. These affinities are significantly tighter than the K_d values of 35 μM and 2 mM reported for *Ps*PBGS (17).

Evaluation of the TgPBGS Quaternary Structure—The molecular mass of recombinant *Tg*PBGS was determined by gel filtration under optimal conditions (see "Materials and Methods"). Comparison with standard marker proteins indicates a molecular mass of ~323-kDa *Tg*PBGS, consistent with an octameric structure (Fig. 3*A*), as observed in other PBGS enzymes (7, 31). Unlike *Hs*PBGS or *Ps*PBGS, however, hexamers were not evident in *Tg*PBGS, even as a shoulder of the main

peak. The allosteric Mg^{2+} ions of octameric PBGS reside at a subunit-subunit interface, and their removal from *Ps*PBGS destabilizes the octamer, resulting in hexamer accumulation (6). Purification of *Pa*PBGS without Mg^{2+} yields a dimeric complex, and dialysis against millimolar levels of Mg^{2+} produces an octameric assembly. Substrate has also been shown to stabilize octameric assembly in PBGS proteins prone to oligomer dissociation (6, 25, 31, 32, 33). Native gel electrophoresis of *Tg*PBGS reveals that this protein is primarily present as an octamer (Fig. 3*B*), and even dialysis to reduce Mg^{2+} to <0.3 Mg^{2+}/octamer does not affect the quaternary structure. The absence of substrate or the presence of EDTA also did not affect the stability of *Tg*PBGS octamer (data not shown).

As noted above, apicomplexan PBGS enzymes are distinguished by their unusual termini, including the N-terminal extension required for targeting to the apicoplast (which is cleaved post-translationally) and C-terminal extension unique to these parasites (*Vibrio cholera* also displays a shorter, unrelated C-terminal extension; supplemental Fig. S1). *Tg*PBGS-ΔC, a mutant form of the enzyme lacking the C-terminal 13 amino acids, purified as dimers according to gel filtration analysis (Fig. 3*A*). The absence of higher order *Tg*PBGS-ΔC oligomers was also confirmed by native gel electrophoresis (Fig. 3*B*) and Western blotting (Fig. 3*C*). This striking difference in the native structure of *Tg*PBGS-wt *versus* *Tg*PBGS-ΔC suggests that the C-terminal 13-amino acid extension may be required for octamer stability. Specific activity of *Tg*PBGS-ΔC was ~25-fold lower than for *Tg*PBGS-wt (~1 μmol/mg protein/h; Fig. 3*D*), but it is not clear if this activity is intrinsic to the dimer or due to transient octamer formation in the presence of substrate, which is known to stabilize the octamer form of PBGS in other species.

In order to further explore the role of the *Tg*PBGS C-terminal extension, we constructed a homology model based on the known structure of *Pa*PBGS (see "Materials and Methods"). Individual PBGS subunits form a ~300-amino acid $\alpha_8\beta_8$-barrel, with an extended N-terminal arm of variable length that interacts with other subunits in oligomeric forms of the enzyme (4). Available crystal structures also show that the C terminus, which is often disordered in the crystal structure, points toward the N terminus and might therefore influence higher order oligomer formation as well. The structural model of *Tg*PBGS (Fig. 3*E*) predicts that the C-terminal extension increases the interaction surface area from 1604 to 2023 Å^2. In addition, the solvation free energy of the protein interface (Δ^iG; calculated by the Protein Interfaces, Surfaces, and Assemblies Service, EBI) was −14.6 kcal/mol for *Tg*PBGS-wt *versus* −4.4 kcal/mol in the *Tg*PBGS-ΔC mutant. For comparison, the average Δ^iG for the equivalent interface in crystal structures of human, mouse, yeast, *Chlorobium*, and *E. coli* PBGS are -15.4 ± 5.4 kcal/mol, strongly arguing that the C-terminal extension of *Tg*PBGS is required for the formation of an energetically favorable interface. This contrasts with *Ps*PBGS and *Pa*PBGS but is consistent with the observation that *Tg*PBGS octamers remain stable in the absence of Mg^{2+} (see above), presumably due to stability provided by the C-terminal extension.

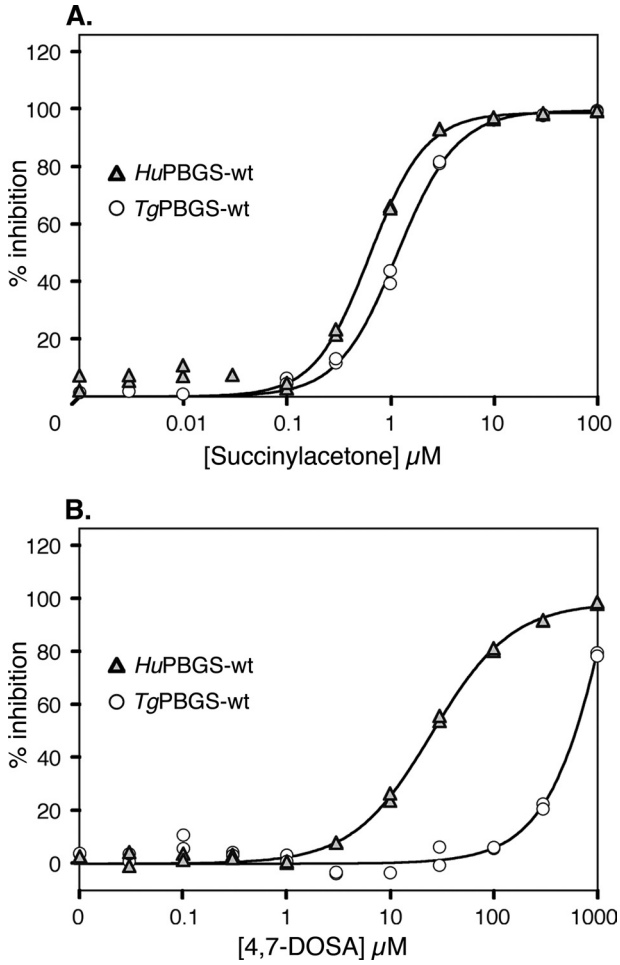

FIGURE 4. **Inhibition of PBGS activity by active site-directed suicide inhibitors.** Inhibition of *Tg*PBGS and *Hs*PBGS enzyme activity (under optimal conditions) by succinylacetone (*A*, preincubated 30 min) or 4,7-dioxosebacic acid (*4,7-DOSA*) (*B*, preincubated 100 min).

Inhibition of TgPBGS and Heme Biosynthesis in T. gondii—Previous studies have described various substrate mimics that specifically inhibit PBGS (28, 34–37, 41), including succinylacetone, which mimics ALA and is a potent irreversible inhibitor (38). As shown in Fig. 4*A*, the dose-response curve for succinylacetone inhibition of *Tg*PBGS is comparable with that of *Hs*PBGS, with IC_{50} values of ~1 μM. This is to be expected because the inhibitor binds covalently to a conserved active site lysine, causing suicide inhibition (39). In contrast, the active site-directed, species-specific irreversible inhibitor 4,7-dioxosebacic acid, which is most effective against Zn^{2+}-requiring PBGS (28, 37, 40), shows ~40-fold selectivity for *Hs*PBGS relative to *Tg*PBGS (Fig. 4*B*). The specificity of 4-oxosebacic acid for *E. coli* PBGS is also understood at a mechanistic level (37, 40, 41); this compound failed to inhibit either *Tg*PBGS or *Hs*PBGS (not shown), even at concentrations as high as 3 mM and a preincubation time up to 24 h.

Robust heme synthesis is observed during active stages of the *T. gondii* life cycle and can be monitored by following the incorporation of ^{14}C-ALA. PBGS enzyme activity in parasite cell lysates was inhibited by succinylacetone in a dose-dependent manner (Fig. 5*A*). Succinylacetone treatment also markedly decreased parasite heme biosynthesis (Fig. 5*B*).

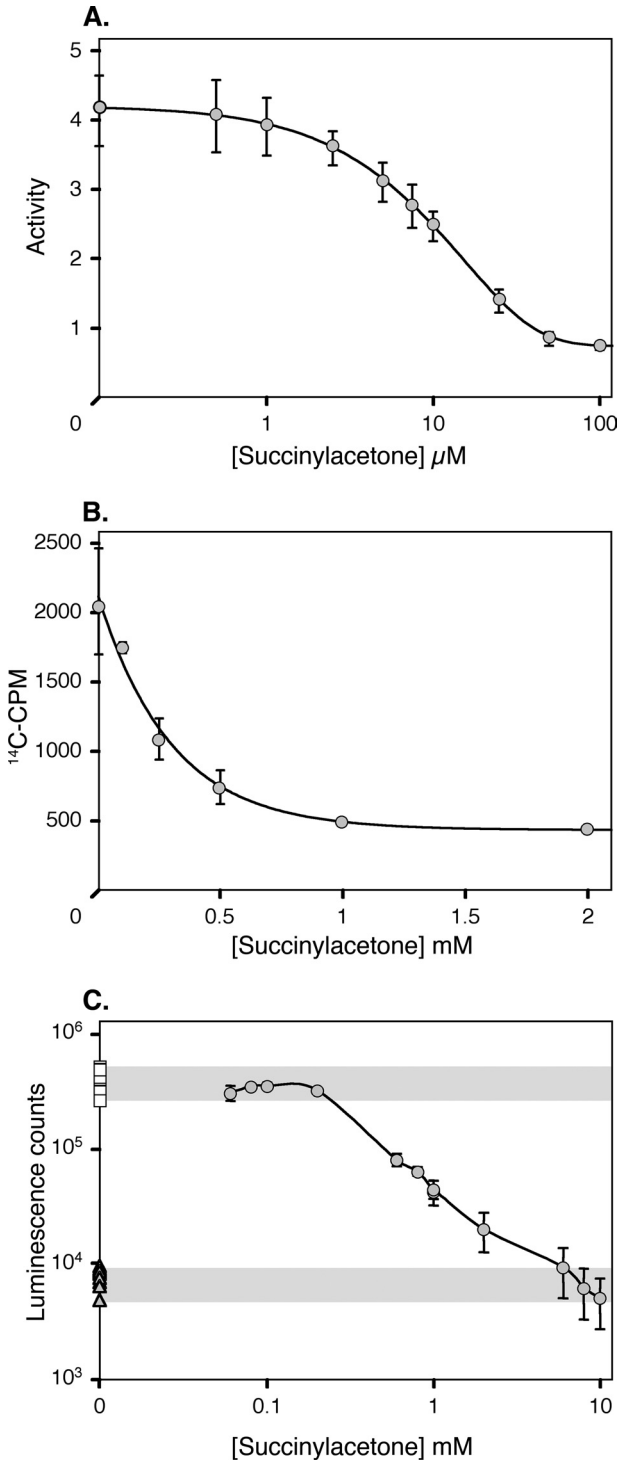

FIGURE 5. **Effect of succinyl acetone on *T. gondii*.** *A*, inhibition of PBGS activity, assayed as porphobilinogen production by *T. gondii* tachyzoite lysates (preincubated 20 min with inhibitor in 100 mM Bistris propane buffer, pH 9.0, at 37 °C prior to 1-h incubation with substrate). *B*, inhibition of heme biosynthesis, assayed as ^{14}C-ALA incorporation into heme by extracellular tachyzoite stage parasites. *C*, inhibition of *T. gondii* growth by succinylacetone. Transgenic parasite tachyzoites expressing luciferase (*circles*) were used to monitor growth in primary human foreskin fibrobast cells. *Shading* indicates positive and negative controls. *Squares*, untreated parasites; *triangles*, parasites lacking the luciferase transgene. *Error bars* indicate standard deviation.

The effect of succinylacetone on the survival of *T. gondii* parasites was monitored using transgenic lines expressing a luciferase reporter gene (15) (Fig. 5*C*). Once again, succinylacetone decreased *T. gondii* growth in a dose-dependent manner, ultimately killing the parasites. Similar dose-response curves were obtained for heme incorporation and parasite survival. Comparable results have been reported previously for *Plasmodium* species (10), suggesting that PBGS activity and heme biosynthesis may be essential for apicomplexan parasite survival.

DISCUSSION

The Unusual PBGS Gene Structure of Apicomplexan Parasites—Heme biosynthesis in *T. gondii* and *P. falciparum* is distinct from their animal hosts in that three enzymes of the common pathway, including PBGS, are located in the apicoplast (12). Motifs required for plastid targeting (42) can be identified in the sequence of *Tg*PBGS and *P. falciparum* PBGS, and apicoplast localization has been confirmed in both species (12, 13, 43). In both species, PBGS sequences (TGME49_053900 and PF14_0381) lie immediately upstream of a stromal processing peptidase gene (pitrilysin; SPP; TGME49_053890 and PF14_0382). These two genes form a single genetic locus, exploiting the same upstream exons to encode an apicoplast-targeting signal (Fig. 1*E*), which is post-translationally removed by signal peptidase and pitrilysin to yield two distinct mature proteins (Fig. 1*A*). At the transcript level, *Tg*PBGS is ~3–5-fold more abundant than *Tg*SPP (Fig. 1*B*); the analogous transcripts in *Plasmodium* are equally abundant (22). Mapping the mature N terminus of *Tg*PBGS confirms that processing occurs near the 3′-end of exon 2, removing most of the sequences shared by *Tg*PBGS and *Tg*SPP (Fig. 1*F*). Three alternatively spliced cDNAs encoding PBGS sequence were identified in *T. gondii* cDNA libraries (Fig. 1*A*), but bioinformatic, RNA, protein, and biochemical analyses indicate that *Tg*PBGS3 is by far the most abundant (Fig. 1*C*) and likely to be the only functional species.

TgPBGS Structure and Function—The activity of recombinant *Tg*PBGS (synthesized without the N-terminal plastid-targeting signals and low complexity sequence; Fig. 1*F*), is comparable with *Hs*PBGS but lower than that reported for *Ps*PBGS. Efforts to express the full-length mature wild type *Tg*PBGS protein (amino acids 148–658) were unsuccessful, probably because of low complexity sequence in the N-terminal region (amino acids 148–301). This domain is not well conserved between *Plasmodium* and *Toxoplasma* or even between *T. gondii* and its close relative *N. caninum.* Several insertions and deletions in the low complexity region are observed in different *T. gondii* isolates. We therefore expect that the *Tg*PBGS-wt protein used for these studies (amino acids 302–658) accurately reflects the enzyme *in vivo*.

Dialysis, EDTA treatment, and Mg^{2+} titration experiments lead us to conclude that *Tg*PBGS requires Mg^{2+}, which is bound very tightly, but that the importance of Mg^{2+} to enzyme quarternary structure differs from that observed in plant/algal PBGS. In *Ps*PBGS, Mg^{2+} is required for activity, binding to both the active site and an allosteric site located at a subunit interface. The latter is required for the assembly of active octamers rather than inactive hexamers (6, 31). Similarly, the removal of

Mg^{2+} from *Pa*PBGS promotes the formation of inactive dimers. Although titration demonstrates the importance of Mg^{2+} for optimal *Tg*PBGS activity (Fig. 2*E*), which was abolished by complete Mg^{2+} removal (Fig. 2*D*), *Tg*PBGS purified in 1 mM $MgCl_2$ retained its octameric structure and ~40% maximal enzyme activity even after removal of Mg^{2+} by dialysis (Fig. 2*C*). Atomic absorption spectroscopy confirmed very low levels of Mg^{2+} ions in dialyzed *Tg*PBGS, but the addition of 10 mM ALA to the assay introduces trace Mg^{2+} that may be sufficient for activity. *Ps*PBGS shows no activity under such conditions because its affinity for Mg^{2+} is much lower (see the legend to Fig. 2*C*). Mg^{2+} concentration in the chloroplast varies between ~1 and 10 mM to support chlorophyll synthesis; although Mg^{2+} concentration in the apicoplast is unknown, it is likely to be far lower because parasites do not synthesize chlorophyll. Tight binding of Mg^{2+} may therefore be necessary for *Tg*PBGS function.

Quaternary structure has been shown to dramatically affect the activity of PBGS from many species (29). The plant and human enzymes are now known to exist as a mixture of low activity hexamers and high activity octamers whose interconversion occurs through a conformational change in the dissociated dimeric assembly. These non-additive quaternary isoforms of the enzyme are called "morpheein forms," and proteins that behave in this fashion are called "morpheeins" (9). Interconversion of morpheein forms requires oligomer disassembly, conformational change in the dissociated state, and reassembly as a structurally and functionally distinct oligomer. The equilibrium of quaternary structure assemblies of PBGS is affected by the presence of metal ions and substrate molecules, both of which favor formation of high activity octamers (7, 25). For *Ps*PBGS, the equilibrium between octamers and hexamers results in a protein concentration dependence of the specific activity. Under optimal conditions, the specific activity of *Tg*PBGS also exhibits protein concentration dependence (Fig. 2*B*), although there is no evidence for hexamers (Fig. 3, *A*–*C*). Thus, the quaternary structure equilibrium for *Tg*PBGS is unlike that of the prototype plant PBGS.

A key structural difference between *Tg*PBGS and *Ps*PBGS is the C-terminal extension present in the former. Protein sequence alignments show that all apicomplexan PBGS enzymes contain such a C-terminal extension, although the precise sequence is not conserved (supplemental Fig. S1). Removal of this sequence in the mutant enzyme *Tg*PBGS-ΔC completely eliminated its ability to assemble beyond the dimeric state (Fig. 3, *A*–*C*), pointing to the C terminus as likely to be responsible for observed differences in quaternary structure equilibria between *Tg*PBGS and other plant-type PBGS enzymes. Fig. 3*E* provides a model suggesting how the C-terminal extension may hold the octamer together. Note that the C-terminal extension is predicted to lie at the edge of PBGS dimers (*blue-green pairs*), interacting with the C-terminal extension of adjacent dimers in an energetically favored conformation. Why *Tg*PBGS might have evolved to use an octamer-stabilizing C-terminal extension whereas allosteric Mg^{2+} is sufficient to stabilize the octameric structure in *Ps*PBGS is unclear but provides scope for further studies on morpheein structure and function and structural differences that might be exploited for therapeutic development. Crystallographic data for *Tg*PBGS would certainly help to expedite these goals.

Capitalizing on Apicomplexan PBGS for Drug Discovery—PBGS is likely to be essential for parasite survival, both by analogy to other systems and based on the observations that treatment with succinylacetone inhibits heme biosynthesis and kills *T. gondii* (albeit only at micromolar concentrations, as also observed in other eukaryotic systems). Most known inhibitors of PBGS are substrate mimics that bind the highly conserved active site, making it challenging to design small molecules that can discriminate between the human and parasite enzymes (although note that 4,7-dioxosebacic acid is far more active against *Hs*PBGS than *Tg*PBGS). Allosteric inhibitors may be more readily developed to exploit phylogenetic differences in protein sequence and structure. Recent studies have demonstrated the potential of species-specific allosteric structure-based inhibitors of PBGS that function by trapping the protein in its inactive hexameric assembly (33, 44). Such inhibitors, termed "morphlocks," have been selected through *in silico* screening for molecules that bind to a phylogenetically variable surface cavity found only in the low activity PBGS hexamer. A similar structure-based approach may be envisioned for discriminating human *versus* parasite PBGS, focusing on the parasite-specific C-terminal domain required for active octamer formation.

Acknowledgments—We acknowledge Linda Stith for technical assistance, Dr. Manami Nishi for assistance with microscopic imaging, Prof. Roland Dunbrack and the Fox Chase Cancer Center Molecular Modeling Facility for assistance with construction of the TgPBGS model, and Prof. Reinhard Neier for 4,7-dioxosebacic acid.

REFERENCES

1. Papenbrock, J., and Grimm, B. (2001) *Planta* **213,** 667–681
2. Heinemann, I. U., Jahn, M., and Jahn, D. (2008) *Arch. Biochem. Biophys.* **474,** 238–251
3. Jaffe, E. K. (2004) *Bioorg. Chem.* **32,** 316–325
4. Jaffe, E. K. (2000) *Acta Crystallogr. D Biol. Crystallogr.* **56,** 115–128
5. Jaffe, E. K. (2003) *Chem. Biol.* **10,** 25–34
6. Breinig, S., Kervinen, J., Stith, L., Wasson, A. S., Fairman, R., Wlodawer, A., Zdanov, A., and Jaffe, E. K. (2003) *Nat. Struct. Biol.* **10,** 757–763
7. Tang, L., Stith, L., and Jaffe, E. K. (2005) *J. Biol. Chem.* **280,** 15786–15793
8. Jaffe, E. K., and Stith, L. (2007) *Am. J. Hum. Genet.* **80,** 329–337
9. Jaffe, E. K. (2005) *Trends Biochem. Sci.* **30,** 490–497
10. Surolia, N., and Padmanaban, G. (1992) *Biochem. Biophys. Res. Commun.* **187,** 744–750
11. Srivastava, P., and Pandey, V. C. (1998) *Exp. Parasitol.* **88,** 60–63
12. Wu, B. (2006) *Heme Biosynthetic Pathway in Apicomplexan Parasites*, Ph.D. thesis, University of Pennsylvania, Philadelphia, PA
13. Dhanasekaran, S., Chandra, N. R., Chandrasekhar Sagar, B. K., Rangarajan, P. N., and Padmanaban, G. (2004) *J. Biol. Chem.* **279,** 6934–6942
14. Roos, D. S., Donald, R. G., Morrissette, N. S., and Moulton, A. L. (1994) *Methods Cell Biol.* **45,** 27–63
15. Matrajt, M., Nishi, M., Fraunholz, M. J., Peter, O., and Roos, D. S. (2002) *Mol. Biochem. Parasitol.* **120,** 285–289
16. Bonday, Z. Q., Taketani, S., Gupta, P. D., and Padmanaban, G. (1997) *J. Biol. Chem.* **272,** 21839–21846
17. Kervinen, J., Dunbrack, R. L., Jr., Litwin, S., Martins, J., Scarrow, R. C., Volin, M., Yeung, A. T., Yoon, E., and Jaffe, E. K. (2000) *Biochemistry* **39,** 9018–9029
18. Canutescu, A. A., and Dunbrack, R. L., Jr. (2005) *Bioinformatics* **21,** 2914–2916

19. Xiang, Z., Soto, C. S., and Honig, B. (2002) *Proc. Natl. Acad. Sci. U.S.A.* **99,** 7432–7437
20. Canutescu, A. A., Shelenkov, A. A., and Dunbrack, R. L., Jr. (2003) *Protein Sci.* **12,** 2001–2014
21. Krissinel, E., and Henrick, K. (2007) *J. Mol. Biol.* **372,** 774–797
22. van Dooren, G. G., Su, V., D'Ombrain, M. C., and McFadden, G. I. (2002) *J. Biol. Chem.* **277,** 23612–23619
23. Seeber, F. (1997) *Parasitol. Res.* **83,** 309–311
24. Roos, D. S., Crawford, M. J., Donald, R. G., Kissinger, J. C., Klimczak, L. J., and Striepen, B. (1999) *Curr. Opin. Microbiol.* **2,** 426–432
25. Jaffe, E. K., Ali, S., Mitchell, L. W., Taylor, K. M., Volin, M., and Markham, G. D. (1995) *Biochemistry* **34,** 244–251
26. Petrovich, R. M., Litwin, S., and Jaffe, E. K. (1996) *J. Biol. Chem.* **271,** 8692–8699
27. Frankenberg, N., Jahn, D., and Jaffe, E. K. (1999) *Biochemistry* **38,** 13976–13982
28. Kervinen, J., Jaffe, E. K., Stauffer, F., Neier, R., Wlodawer, A., and Zdanov, A. (2001) *Biochemistry* **40,** 8227–8236
29. Selwood, T., Tang, L., Lawrence, S. H., Anokhina, Y., and Jaffe, E. K. (2008) *Biochemistry* **47,** 3245–3257
30. Bollivar, D. W., Clauson, C., Lighthall, R., Forbes, S., Kokona, B., Fairman, R., Kundrat, L., and Jaffe, E. K. (2004) *BMC Biochem.* **5,** 17
31. Kokona, B., Rigotti, D. J., Wasson, A. S., Lawrence, S. H., Jaffe, E. K., and Fairman, R. (2008) *Biochemistry* **47,** 10649–10656
32. Jaffe, E. K. (1995) *J. Bioenerg. Biomembr.* **27,** 169–179
33. Lawrence, S. H., Ramirez, U. D., Tang, L., Fazliyez, F., Kundrat, L., Markham, G. D., and Jaffe, E. K. (2008) *Chem. Biol.* **15,** 586–596
34. Senior, N. M., Brocklehurst, K., Cooper, J. B., Wood, S. P., Erskine, P., Shoolingin-Jordan, P. M., Thomas, P. G., and Warren, M. J. (1996) *Biochem. J.* **320,** 401–412
35. Gacond, S., Frère, F., Nentwich, M., Faurite, J. P., Frankenberg-Dinkel, N., and Neier, R. (2007) *Chem. Biodivers.* **4,** 189–202
36. Heinemann, I. U., Schulz, C., Schubert, W. D., Heinz, D. W., Wang, Y. G., Kobayashi, Y., Awa, Y., Wachi, M., Jahn, D., and Jahn, M. (2010) *Antimicrob. Agents Chemother.* **54,** 267–272
37. Jarret, C., Stauffer, F., Henz, M. E., Marty, M., Lüönd, R. M., Bobálová, J., Schürmann, P., and Neier, R. (2000) *Chem. Biol.* **7,** 185–196
38. Tschudy, D. P., Hess, R. A., and Frykholm, B. C. (1981) *J. Biol. Chem.* **256,** 9915–9923
39. Erskine, P. T., Newbold, R., Brindley, A. A., Wood, S. P., Shoolingin-Jordan, P. M., Warren, M. J., and Cooper, J. B. (2001) *J. Mol. Biol.* **312,** 133–141
40. Erskine, P. T., Coates, L., Newbold, R., Brindley, A. A., Stauffer, F., Wood, S. P., Warren, M. J., Cooper, J. B., Shoolingin-Jordan, P. M., and Neier, R. (2001) *FEBS Lett.* **503,** 196–200
41. Jaffe, E. K., Kervinen, J., Martins, J., Stauffer, F., Neier, R., Wlodawer, A., and Zdanov, A. (2002) *J. Biol. Chem.* **277,** 19792–19799
42. Waller, R. F., Keeling, P. J., Donald, R. G., Striepen, B., Handman, E., Lang-Unnasch, N., Cowman, A. F., Besra, G. S., Roos, D. S., and McFadden, G. I. (1998) *Proc. Natl. Acad. Sci. U.S.A.* **95,** 12352–12357
43. Sato, S., Clough, B., Coates, L., and Wilson, R. J. (2004) *Protist* **155,** 117–125
44. Lawrence, S. H., Ramirez, U. D., Selwood, T., Stith, L., and Jaffe, E. K. (2009) *J. Biol. Chem.* **284,** 35807–35817